AGU PUBLICATIONS

JGR

Journal of Geophysical Research: Space Physics

RESEARCH ARTICLE

10.1002/2016JA022969

Key Points:
- Jupiter chorus intensity is binned in f, L, latitude, and MLT
- Parametric fits of intensity versus frequency and latitude determined
- Spatial range of chorus emissions is extended from previous work

Correspondence to:
J. D. Menietti,
john-menietti@uiowa.edu

Citation:
Menietti, J. D., J. B. Groene, T. F. Averkamp, R. B. Horne, E. E. Woodfield, Y. Y. Shprits, M. de Soria-Santacruz Pich, and D. A. Gurnett (2016), Survey of whistler mode chorus intensity at Jupiter, *J. Geophys. Res. Space Physics*, *121*, 9758–9770, doi:10.1002/2016JA022969.

Received 18 MAY 2016
Accepted 27 SEP 2016
Accepted article online 29 SEP 2016
Published online 19 OCT 2016

Survey of whistler mode chorus intensity at Jupiter

J. D. Menietti[1], J. B. Groene[1], T. F. Averkamp[1], R. B. Horne[2], E. E. Woodfield[2], Y. Y. Shprits[3,4], M. de Soria-Santacruz Pich[5], and D. A. Gurnett[1]

[1]University of Iowa, Department of Physics and Astronomy, Iowa City, Iowa, USA, [2]British Antarctic Survey, Cambridge, UK, [3]Department of Earth and Space Sciences, University of California, Los Angeles, California, USA, [4]Department of Earth, Atmospheric and Planetary Sciences, MIT, Cambridge, Massachusetts, USA, [5]Jet Propulsion Laboratory, California Institute of Technology, Pasadena, California, USA

Abstract Whistler mode chorus emission is important in the acceleration of electrons and filling of the radiation belts at Jupiter. In this work chorus magnetic intensity levels (frequency-integrated spectral density, P_B) at Jupiter are comprehensively binned and parameterized. The frequency range of chorus under study extends from the lower hybrid frequency, f_{lh}, to $f_{ceq}/2$ and $f_{ceq}/2 < f < 0.8\ f_{ceq}$, where f_{ceq} is the cyclotron frequency mapped to the magnetic equator. The goal is to obtain a quantized distribution of magnetic intensity for use in stochastic modeling efforts. Parametric fits of magnetic plasma wave intensity are obtained, including P_B versus frequency, latitude, and L shell. The results indicate that Jupiter chorus occurrence probability and intensity are higher than those at Saturn, reaching values observed at Earth. Jovian chorus is observed over most local times, confined primarily to the range $8 < L < 15$, outside the high densities of the Io torus. The largest intensity levels are seen on the dayside; however, the sampling of chorus on the nightside is much less than on the dayside. Peak intensities occur near the equator with a weak dependence on magnetic latitude, λ. We conclude that Jovian chorus average intensity levels are approximately an order of magnitude lower than those at Earth. In more isolated regions the intensities are comparable to those observed at Earth. The spatial range of the chorus emissions extends beyond that assumed in previous Jovian global diffusive models of wave-particle electron acceleration.

1. Introduction

Comparative studies of planetary magnetospheres are important to fully understand the dynamical processes at work in the different environments, for instance, a solar wind controlled magnetosphere at Earth compared to one that is rotationally controlled as at Jupiter. How do such differences influence the scattering and acceleration of electrons and the filling of radiation belts, as well as the auroral processes that control radio emission and ionospheric coupling? Comparative studies may also help us to understand the critical parameters and scaling laws that determine the behavior of plasma populations in the solar system and beyond.

Whistler mode chorus emission is known to be a significant source of electron energization at Earth [*Horne and Thorne*, 1998, 2003; *Horne et al*., 2005; *Thorne et al*., 2013, and references therein]. Chorus emission distribution at Jupiter has been studied in the past [*Hospodarsky et al*., 2008, 2012; *Menietti et al*., 2008b, 2012; *Katoh et al*., 2011]. The potential importance of chorus emission for the acceleration and loss of relativistic electrons at Jupiter has been shown [*Horne et al*., 2008], but this study was based on preliminary chorus measurements. Subsequent studies showed that the results of the simulations are sensitive to the assumed parameters of chorus waves [*Shprits et al*., 2012; *Woodfield et al*., 2013, 2014]. An extensive survey of Jovian chorus intensity as a function of frequency and spatial parameters has not previously been presented. In order to conduct modeling of pitch angle and energy scattering of electrons by chorus emission at the outer planets, knowledge of chorus occurrence rates and intensity levels is essential, as well as the spatial distribution of this intensity.

Chorus emission at Earth is generated near the magnetic equator, just outside the plasmapause in regions of lower ratio of plasma to cyclotron frequency, f_p/f_c, with a free energy source of plasma injections of tens of keV electrons. This process along with convection leads to a region of high occurrence of chorus at Earth that extends from the nightside through dawn to near-noon local time [*Thorne*, 2010; *Santolík et al*., 2010]. At Jupiter chorus is believed to have a source near the magnetic equator [*Menietti et al*., 2008a; *Hospodarsky et al*., 2012]. The typical frequency range of chorus is several hundreds of hertz to

several kilohertz [cf. *Menietti et al*., 2008, Figure 2; *Menietti et al*., 2012, Figure 3]. The free energy source of this chorus may be associated with warm plasma within inward convecting magnetic flux tubes associated with the interchange instability in a corotation-dominated magnetosphere [*Hill et al*., 1983; *Pontius et al*., 1986; *Thorne et al*., 1997; *Bolton et al*., 1997]. Enhancement of chorus within such regions at Saturn has been shown [*Hospodarsky et al*., 2008; *Menietti et al*., 2008b]. Other electron free energy sources of chorus emission at Jupiter may result from plasma injection events [*Mauk et al*., 1997, 1999], magnetic compression events [*Cowley and Bunce*, 2003], and magnetic reconnection [*Louarn et al*., 2014].

In this paper an extensive survey of the chorus intensity levels at Jupiter is presented using Galileo plasma wave data, and fits of the intensity as a function of relative frequency, magnetic latitude, *L* shell, and distribution in local time are performed. The empirical models of the Jovian wave environment can be useful in future stochastic modeling of electron scattering and acceleration.

2. Methodology

The general scheme for conducting the chorus survey is similar to that presented in *Menietti et al.* [2014] for observations at Saturn. We introduce spatial bins in magnetic *L* shell (*L*), magnetic local time (MLT), and magnetic latitude (λ). Whistler mode chorus is assumed to be generated close to the magnetic equator and to propagate close to the magnetic field. The frequency spectrum for chorus was determined for the upper and lower bands normalized to the cyclotron frequency mapped to equator, f_{ceq}, ranging over $f_{min} < f < f_{ceq}/2$ and $f_{ceq}/2 < f < 0.8 f_{ceq}$, where $f_{min} > f_{lh}$ is the minimum frequency determined by examination to be above low-frequency noise and interference and f_{lh} is the lower hybrid frequency at the equator. This frequency was typically less than 200 Hz for the first 10 orbits. Beginning at orbit 11, f_{min} was increased to typically 350 Hz until orbit 15 when the value was again increased in the range 600–2700 Hz due to increased noise levels of the magnetic receivers. The lower band chorus is divided into five frequency bins and the upper band into three frequency bins. We introduce relative frequency, $\beta_i = f_i/f_{ceq}$, where f_i is the center frequency of the frequency bin, $\Delta\beta_i$. For the lower band we define $f_{lh}/f_{ceq} < \Delta\beta_1 < 0.1$, $0.1 < \Delta\beta_2 < 0.2$, $0.2 < \Delta\beta_3 < 0.3$, $0.3 < \Delta\beta_4 < 0.4$, and $0.4 < \Delta\beta_5 < 0.5$, while for the upper band with fewer channels available we define $0.5 < \Delta\beta_6 < 0.6$, $0.6 < \Delta\beta_7 < 0.7$, and $0.7 < \Delta\beta_8 < 0.8$. The wave magnetic intensity, P_B, is proportional to $B^2(\mathrm{nT}^2)$. From the measured magnetic spectral density, $\chi(f)$, in units of $\mathrm{nT}^2/\mathrm{Hz}$, over a range of frequencies, we determine $B^2(\beta_i)$ (measured in nT^2) by integration over the frequency channels within $\Delta\beta_i$ for a time step, $\Delta\tau$ (typically 32 s, the time required to scan the low-, medium-, and high-frequency channels, once for the electric and once for the magnetic antennas). We note that the time steps within $\Delta\tau$ for individual $\Delta\beta_i$ within the medium frequency receiver (MFR) are much smaller than 32 s (there are 112 frequency channels within the MFR). The sum of these integrations is what we call P_{Bi}. The spacecraft position (*L*, λ, and MLT) at each time step, $\Delta\tau$, is always recorded. When seeking $P_B(\beta)$, we calculate the mean value of P_B within any chosen spatial bin (ΔL, ΔMLT, and $\Delta\lambda$) by averaging all P_{Bi} within that spatial bin during the total integration time (the sum of $\Delta\tau$). For a specific ΔL, by calculating averages over all values of MLT, and all values of λ, we can then fit $P_B(\beta)$ to a functional form $P_B(\beta) = P_o\, 10^{m\beta}$ and determine the fitting parameters P_o, m, and β.

We calculate the value of P_B per spectrum, P_{Bs}, by summing all the P_{Bi} for either the lower or upper bin for each $\Delta\tau$. If we wish to obtain P_B for a specified spatial range, we obtain the mean of all P_{Bs} within that spatial range during the total integration time (the sum of all $\Delta\tau$). For instance, to obtain $P_B(\lambda)$, we calculate these mean values within a specific ΔL for all values of MLT and for all values of λ within each bin of latitude, $\Delta\lambda$. It is then possible to fit to the functional form $P_B(\lambda) = P_o\, 10^{m\lambda}$.

For calculations of P_B versus β, we always obtain the average of all P_{Bi} for each relative frequency bin within a spatial bin. For calculations of P_B versus spatial coordinates we always obtain the average of all P_{Bs} for either the lower or upper bin within a spatial bin as required for the quasi-linear calculation of the scattering rates [*Kennel and Engelmann*, 1966; *Lerche*, 1968].

3. Models and Data Constraints

In order to perform the magnetic mapping of the locally measured values of f_c and f_p (plasma frequency) to the equator, we use the VIP4 magnetic field model with current sheet [*Connerney et al*., 1982, 1983] for

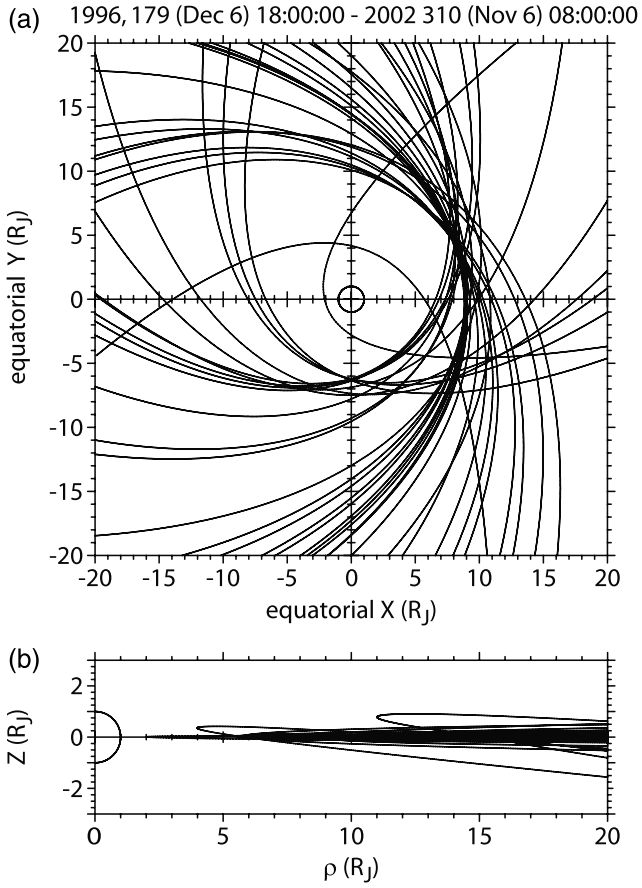

Figure 1. Orbital trajectories in the equatorial (a) *x*-*y* and (b) ρ-z planes of the Galileo spacecraft during the data period, where ρ is the projection of the distance from Jupiter in the equatorial plane. The included dates of the orbital survey are shown.

Jupiter. The plasma density is measured locally by observation of the upper hybrid resonance, $f_{uh} = \sqrt{\left(f_p^2 + f_c^2\right)}$, where f_p is the local plasma frequency. However, when the upper hybrid density is not observed, we use interpolated values of the analytic density model of *Divine and Garrett* [1983]. The model values of the magnetic field and plasma density at the equator are scaled by the locally measured values $n_{eq} = n\ (n'_{eq}/n')$ and $B_{eq} = B\ (B'_{eq}/B')$ where n and B are the locally measured values of plasma density and ambient magnetic field, respectively, and the primed values are the model values. Subscript "eq" refers to the value at the equator. Observed values of the local ambient magnetic field were obtained from the Galileo Magnetic Field Investigation fluxgate measurements [*Kivelson et al.*, 1992].

For Jupiter measurements we use data from the Galileo plasma wave investigation (PWI) [*Gurnett et al.*, 1992]. For this instrument low-time resolution survey electric and magnetic field data were acquired by the low-, medium-, and high-frequency receivers. The electric dipole antenna is 6.6 m long, perpendicular to the spin axis, and there are two orthogonal magnetic search coils also perpendicular to the spin axis. For this study the medium frequency receiver, MFR (42.1 Hz–160.8 kHz), was the principle receiver and the search coil optimized for frequencies up to 50 kHz was used. The time resolution can be either 18.67 or 37.33 s for a full spectral sweep, with $\Delta f/f \sim 8\%$. The magnetic search coils degraded severely after the first 10 orbits of Galileo. For the remainder of the mission (orbits 11 to 34) the electric field data only were used in this survey and the magnetic power was evaluated indirectly from the measured cold plasma refractive index as developed, for example, in chapter 1 of *Stix* [1992] (cf. equation (34)),

$$\eta^2 = 1 - f_p{}^2/[f(f + f_c)] \tag{1}$$

where we have assumed an electron plasma with wave normal angle = 0°. For these orbits we have evaluated the magnetic power spectral density,

$$\chi_B = \chi_E \eta^2/c^2 \tag{2}$$

where χ_E is the measured electric field power spectral density. It is also for this reason that f_{min} was increased at this time. We have compared the value of χ_B obtained directly from observations during the first 10 orbits to the value obtained from equation (2) using χ_E. The comparison is difficult due to the different background thresholds for the electric and magnetic receivers and because of the dependence of the index of refraction on frequency and local plasma parameters (f_p, f_c). Similar to the results of *Hartley et al.* [2015], we found that a majority of the time the cold plasma dispersion relation underestimates the whistler mode intensity levels by a value of up to 2 to 3, with better agreement at higher frequencies. However, during many intervals of more

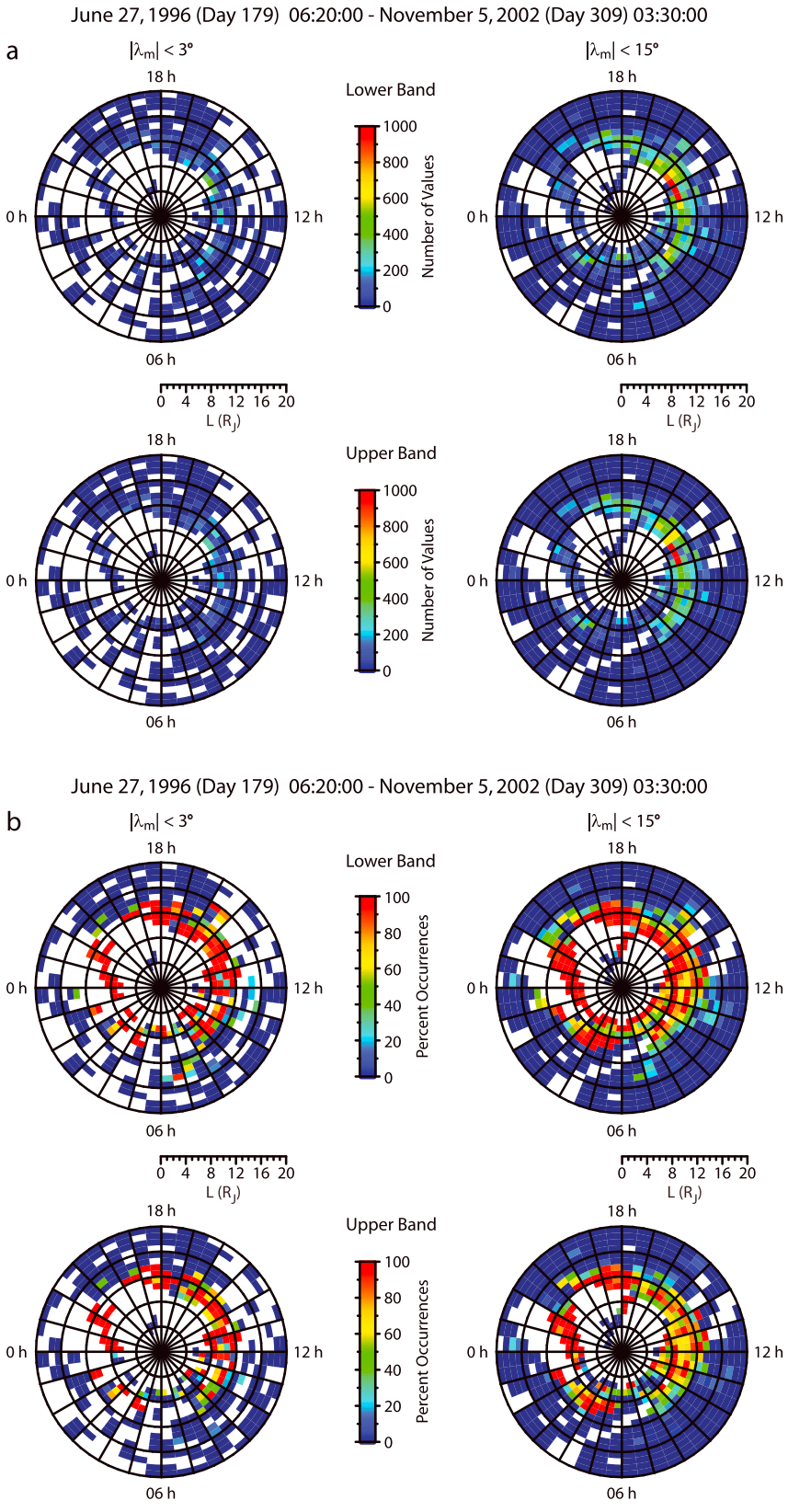

Figure 2. (a) Contour plots in the *L*-MLT plane with the number of chorus spectra observed, N_s, color coded for each bin ($\Delta L = 0.5$) for two latitudes ranges, $|\lambda| < 3°$ and $|\lambda| < 15°$, for the lower and upper bands. (b) Chorus occurrence probability for the same latitude ranges for the lower and upper bands.

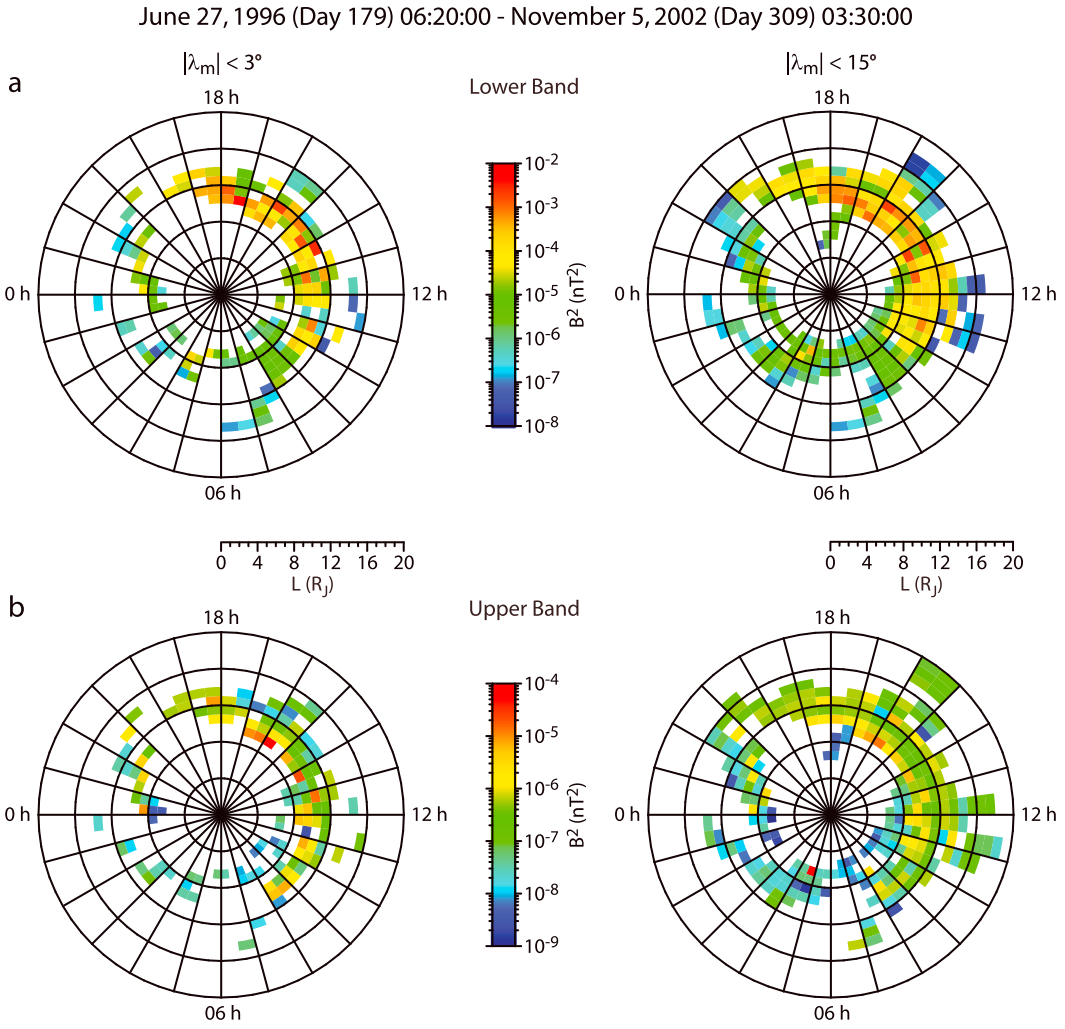

Figure 3. (a) Average chorus intensity in each bin ($\Delta L = 0.5$, ΔMLT = 0.5 h) for the equatorial region, $|\lambda| < 3°$, and over the extended range of latitude to $0 < |\lambda| < 15°$ for each bin ($\Delta L = 0.5$, ΔMLT = 0.5 h). Results are for the (Figure 3a) lower and (Figure 3b) upper bands.

intense emission, the underestimate was an order of magnitude or greater. So it is fair to say that the average intensity levels calculated in this study are a lower limit.

To avoid spacecraft and instrumental interference as well as natural wave interference, a number of constraints were placed on the data analyzed in this survey. Among the more important for the Galileo PWI data are the following constraints set by visually examining the data: (1) A variable (dependent on time), f_{min}, to avoid instrumental noise and low-frequency interference and (2) a variable, χ_{min}, the minimum threshold spectral density (dependent on time and frequency), to avoid background noise (due to instrument calibration, spacecraft and instrument interference, and receiver degradation). These values lie in the ranges $10^{-13} < \chi_{E\min} < 10^{-11}$ ($V^2\,m^{-2}\,Hz^{-1}$) and $10^{-9} < \chi_{B\min}\,10^{-7}$ ($nT^2\,Hz^{-1}$).

3.1. Data Collecting

Menietti et al. [2008a] have reported an earlier survey of the Galileo chorus data. We have expanded that survey by proceeding with the same approach used at Saturn as described above (also, cf. *Meredith et al.* [2012] for Earth studies). The data were collected over more than a 6 year period extending from 27 June 1996 to 5 November 2002. In Figures 1a and 1b we present the inner orbit trajectories in the Jovigraphic equatorial (not magnetic) *x-y* and ρ-*z* planes of the Galileo spacecraft during the data period, where ρ is the projection of the

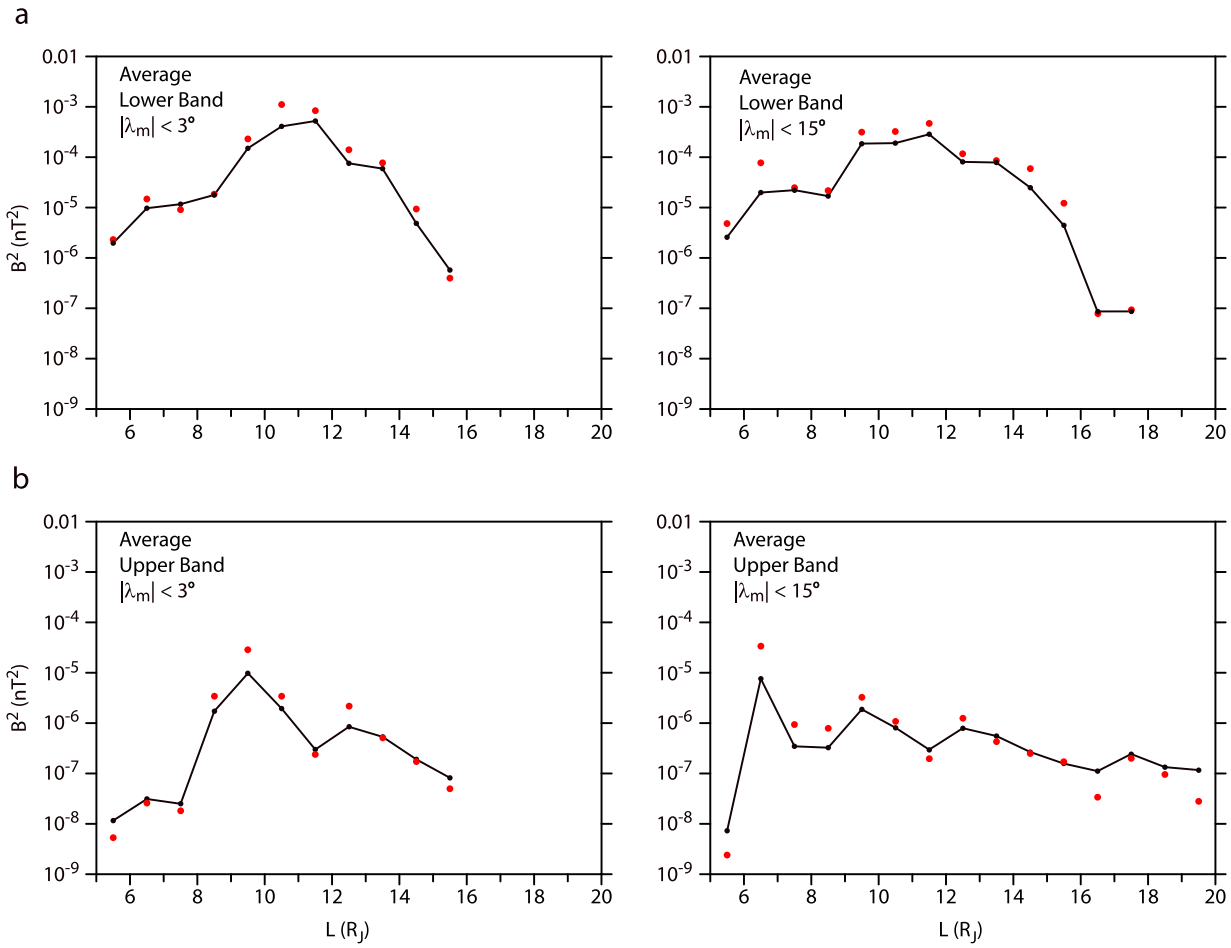

Figure 4. Average chorus intensity as a function of *L*. Red dots are the standard deviation or uncertainty of each point. (a) Average lower band intensity. (b) Intensity levels for the upper band chorus are more than an order of magnitude lower than the lower band chorus.

distance from Jupiter in the equatorial plane. One can see that the orbit coverage in local time is not extensive, especially on the nightside, but where sampling occurs, there can be high occurrence rates of chorus. The Galileo spacecraft orbit plane was close to the Jovigraphic equator, so sampling of magnetic latitudes $|\lambda| < 15°$ was possible due to the tilt of the magnetic axis.

In Figure 2 we display polar contour plots in the *L*-MLT plane. In Figure 2a the number of chorus spectra observed, N_s, within each bin ($\Delta L = 1.0$) for two ranges of magnetic latitudes $|\lambda| < 3°$ and $|\lambda| < 15°$ is shown for the lower and upper bands. N_s is the number of time steps containing intensity levels that lie above the intensity threshold, χ_{min}, and within the frequency range specified at that time. The numbers range from a few to multiple hundreds for each band. In Figure 2b we plot the ratio of the time during which chorus is observed, T_{chorus}, to the total time spent by the spacecraft, in each bin, T_{total}, for the same latitude range, which indicates the occurrence probability of chorus at Jupiter. The boxes are white if the spacecraft did not visit that region. If the spacecraft visited a region (bin), but no chorus was observed, then the intensity was set to zero (dark blue). For the general survey, during each time step, $\Delta\tau$, all relative frequency bins, β_i,

Table 1a. Number of Averaged $\lambda < 3°$ Values for Bins of Figure 4

	$\lambda < 3°$										
L	5.5	6.5	7.5	8.5	9.5	10.5	11.5	12.5	13.5	14.5	15.5
Lower band	148	616	785	867	3302	1733	1525	1326	635	367	225
Upper band	100	323	448	820	2331	1689	1514	1088	369	105	6

Table 1b. Number of Averaged $\lambda < 15°$ Values for Bins of Figure 4

	$\lambda < 15°$												
L	5.5	6.5	7.5	8.5	9.5	10.5	11.5	12.5	13.5	14.5	15.5	16.5	17.5–19.5
Lower band	1166	3987	3593	4268	12804	8101	6773	4697	3094	1534	696	89	<50
Upper band	461	2045	2181	3653	10068	6908	6658	3292	1441	676	63	29	<50

are sampled, and a value of intensity, P_{Bs}, is determined. From Figures 2a and 2b it is clear that there is considerably less coverage on the nightside. The chorus occurrence ratio varies from 0 to 1, and chorus occurrence probabilities > 0.5 for the lower and upper bands of chorus are frequent, indicating nearly a continuous free energy source for chorus generation through much of the Jovian magnetosphere.

3.2. Chorus Intensity Survey

In Figure 3a we display the average chorus intensity (nT^2) in each bin ($\Delta L = 1.0$, $\Delta MLT = 0.5$ h) for the equatorial region, $|\lambda| < 3°$. Note that in Figure 3 (and distinct from Figure 2) if no chorus was observed in a bin or if that bin was not visited, it is white. Chorus intensity is clearly greater on the dayside, but this may be due to the orbital sampling (compare to Figure 2). Nearer the equator the intensity levels peak near 10^{-2} nT^2. There is a rather broad band of moderate intensity in the range ~$8 < L <$ ~ 12 on the dayside, with scattered coverage on the nightside and lower intensity levels. In the right panel we average over the extended range of latitude to $0 < |\lambda| < 15°$ for each bin ($\Delta L = 1.0$, $\Delta MLT = 0.5$ h). The intensity levels again peak near 10^{-2} nT^2, but the range in *L* extends to ~$6 < L <$ ~18 particularly on the dayside, with scattered coverage on the nightside at lower intensity levels. Intensity results for the upper band emission are shown in Figure 3b with peak values approximately 2 orders of magnitude lower than for the lower band.

In the analyses that follow we will plot the chorus intensity as a function of β, *L*, and λ. We will increase the size of the spatial bins compared to those used in Figures 2 and 3 and perform averages of P_{Bi} and P_{Bs} over much larger bins to improve statistics and to better parameterize the data.

3.3. Intensity Versus *L* Shell

In Figure 4 we plot P_B averaged over all magnetic local times and all latitudes for each $\Delta L = 1.0$ in the range $5.0 < L < 20.0$. The number of values averaged in each bin of Figure 4 is listed in Tables 1a and 1b. In Figure 4a the average values for the lower band are shown, and the standard deviation, σ, or square root of the variance is plotted for each point as a red dot. There is a general increase in the chorus intensity to moderate levels, peaking around $L = 12$. In Figure 4b the intensity levels for the upper band chorus are more than an order of magnitude lower than the lower band chorus, but the general trends as a function of *L* are similar to the lower band, but the peak at $L \sim 12$ is shifted lower to $L \sim 10$.

3.4. Intensity Versus Magnetic Latitude

In Figure 5a we present plots of average lower band chorus intensity as a function of magnetic latitude for different ranges of *L*. For a selected range of *L* we average the chorus intensity for all spectra within a spatial bin that includes all magnetic local times within each latitude bin ($\Delta\lambda = 2°$). The maximum spacecraft latitude is less than 15°, and the range of *L* is noted on each plot. Table 2 lists the number of values averaged in each bin of Figure 5. We have also calculated weighted fits of these data to the fitting function $B^2 = A\ 10^{m|\lambda|}$ (fitting parameters are on the figure) and plotted them along with the standard deviation (red dots) of each point. In Figure 5a the panel for $13 < L < 16$ also includes the distribution of values in each bin to demonstrate the range, which is similar for the other panels as well. The standard deviations are large due to the bursty nature of the whistler mode emission, large frequency range, and due to the large number of points at low intensity levels. Increasing the threshold for background emission would decrease the value of σ. All of the plots show a weak dependence of chorus intensity as a function of latitude, with the average levels remaining reasonably constant. In Figure 5b we display the latitude dependence of the upper band chorus, which is about 2 orders of magnitude weaker than the lower band, and also shows a weak dependence on latitude. For the range $4 < L < 7$ there is an anomalous point at $\lambda = 9°$. This point is due to a strong intensity whistler mode event at higher than usual latitude. It may be due to episodic conditions such as a magnetospheric compression or electron injection episode [cf. *Bolton et al.*, 1997]. Since all the points are weighted by σ, the fit is not

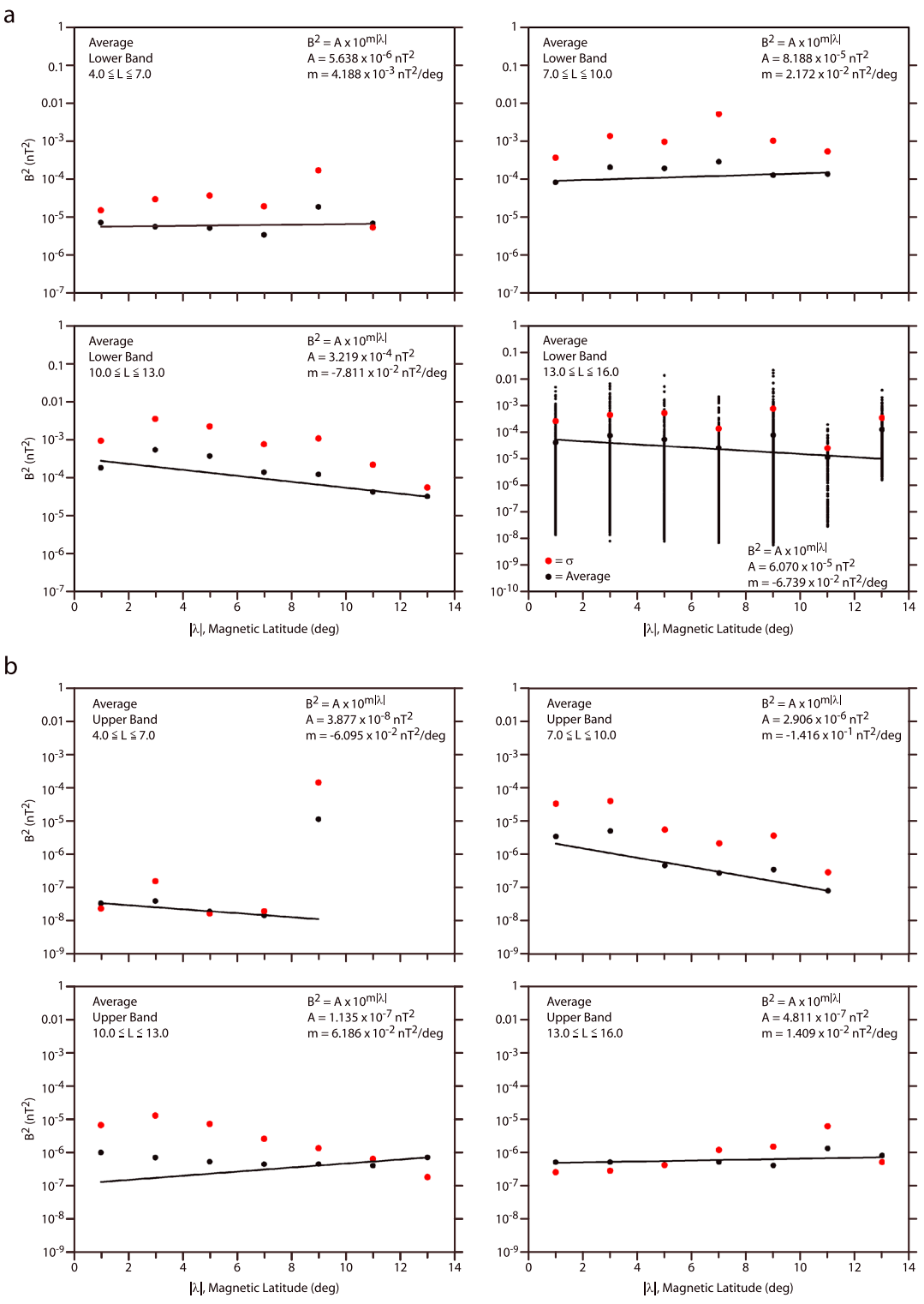

Figure 5. Average chorus intensity as a function of latitude for different ranges of *L*. The range of *L* and fitting function and parameters is noted on each plot. Red dots are the standard deviation of each point. (a) Lower band chorus. The last panel displays the data distribution within each bin. (b) Upper band chorus, which is considerably less intense.

Table 2. Number of Averaged Values for Bins of Figure 5

λ	$4 < L < 7$	$7 < L < 10$	$10 < L < 13$	$13 < L < 16$
		Lower Band		
1.0	558	3339	3202	907
3.0	668	3227	3261	856
5.0	853	3300	3769	926
7.0	1154	3959	3898	1014
9.0	1825	6552	6142	1718
11.0	96	415	416	165
13.0	0	0	18	257
		Upper Band		
1.0	266	2376	2875	331
3.0	326	2410	3096	369
5.0	414	2536	3429	457
7.0	703	3136	3458	521
9.0	857	5071	5759	1114
11.0	0	394	309	104
13.0	0	0	18	257

strongly influenced by the anomalous point. Again, it should be noted that Galileo measurements are limited to ~15° magnetic latitude, and the dependence at higher latitudes is likely to be different.

3.5. Intensity Versus Frequency (β)

From these data we also determine the dependence of chorus intensity on $\beta = f/f_{ceq}$. We select a range of L and calculate the average of P_B for all spectra within a spatial bin that includes all local times and all latitudes. Chorus intensity versus β for each range of L ($\Delta L = 2$) is shown for the lower and upper bands, respectively, in Figures 6 and 7. The fitting function is $B^2 = \mathrm{A}\ 10^{m\beta}$, and the fitting parameters are shown on the figures. The slopes are typically small and negative. The plasma wave data are not typically narrow banded, as is terrestrial chorus, and cannot generally be fit to a Gaussian. We display plots of intensity versus β for $|\lambda| < 3°$ in Figure 6a and data for $|\lambda| < 15°$in Figure 6b. The upper band chorus is limited by the data to three levels, $\beta = 0.55$, 0.65, and 0.75 in Figure 7, with intensity levels 1 or 2 orders of magnitude lower than the lower band.

4. Summary and Conclusions

We have presented a survey of chorus and whistler mode intensity with parametric fits to f, L, λ, and MLT of the Jovian magnetosphere. While the standard deviations of many of the points used to calculate the fits are large, the parametric fits can be useful when used with due consideration of large values of σ. The results will be important for modeling the impact of wave-particle interactions at Jupiter, particularly regarding electron acceleration and the filling of the radiation belts.

The Jovian chorus intensity is obtained from the plasma wave instrument (PWI) on board the Galileo spacecraft over approximately 35 orbits. The majority of time was spent on the dayside, and all observations were limited to $|\lambda_m| < 15°$. The spacecraft sampled all magnetic local times within $4 < r < 20\ R_J$ but not all radial distances. In particular, there is a lack of sampling on the Jovian local nightside, so no firm conclusions can be drawn about the relative strength of nightside to dayside chorus intensity levels. It is possible that within the rotationally controlled Jovian magnetosphere with the plasma flux interchange instability providing a major source of radial transfer, that chorus-free energy electron source populations are found more frequently near the equator on the Jovian dayside rather than on the nightside as at Earth.

The results indicate that chorus and whistler mode emission intensity levels are significant at Jupiter. The chorus intensity is stronger on the dayside, perhaps due to preferential sampling. Average intensity levels peak at a few 10^{-4} nT^2 approaching 10^{-3} nT^2 in the range $10 < L < 12$ (see Figures 4 and 5), which is within an order of magnitude of the average peak chorus intensity at Earth [*Meredith et al*., 2012]. Figure 3 shows that for more isolated regions of integration in the Jovian magnetosphere, chorus levels can be even larger, approaching 10^{-2} nT^2. The upper band emissions have a similar spatial distribution but with intensity levels often 2 orders of magnitude below lower band emission.

The Galileo mission targeted Jovian moon encounters on each orbit for special study, and thus, the sampling of the Jovian magnetosphere has a level of bias. Ganymede, with its intrinsic magnetic field, is unique, and intense chorus is observed during each flyby [*Gurnett et al*., 1996; *Kurth et al*., 1997]. Since the encounter data are confined to the immediate vicinity of this Jovian moon (within at most 2 moon radii), we did not include them in this general survey of chorus emission. Even so, the orbital period of Ganymede is 7.16 days, while the synodic period of Jupiter's rotation is ~ 10.5 h. This, along with radial transport and convective flows,

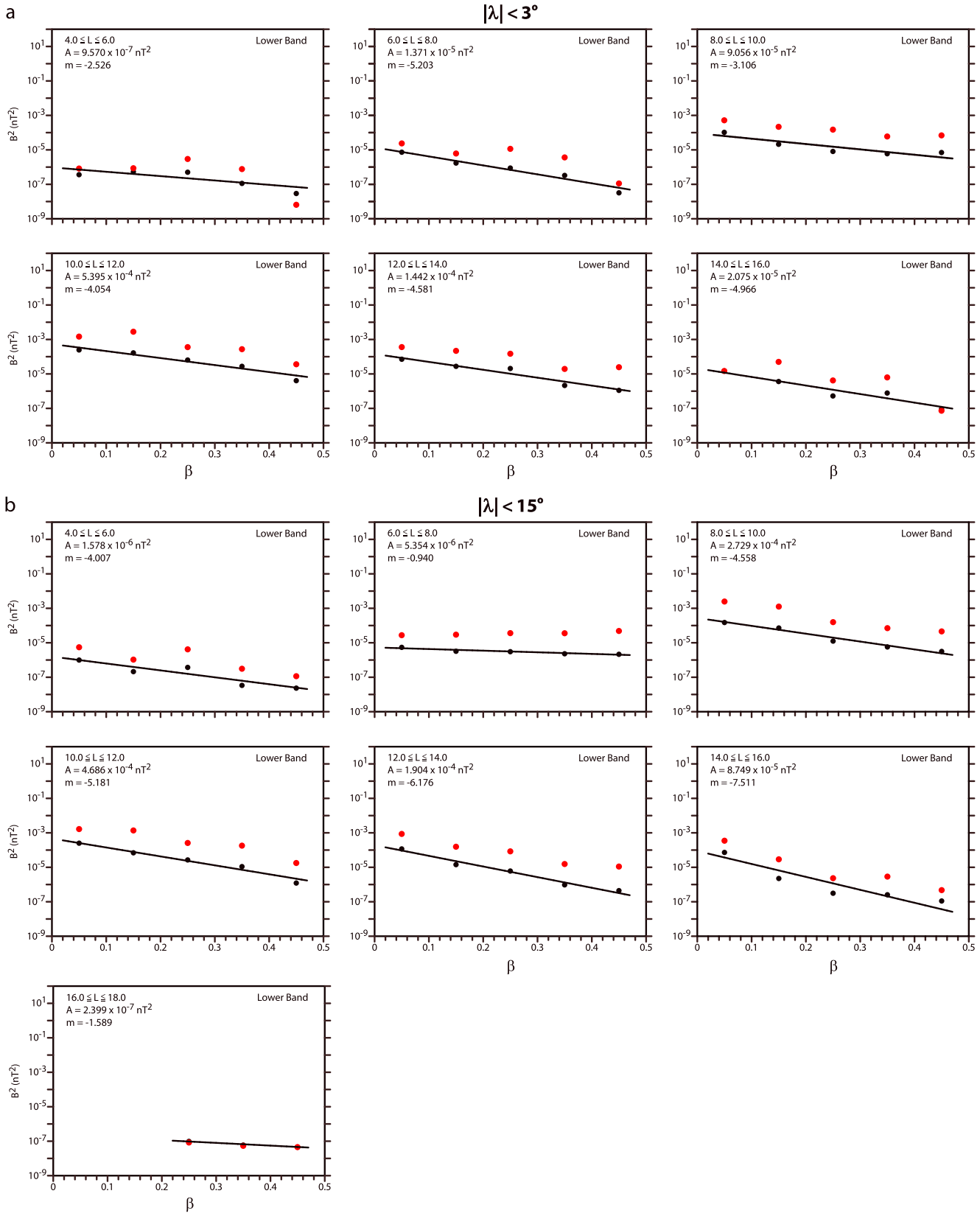

Figure 6. Chorus intensity versus β for each range of L is shown. The fitting function and fitting parameters are shown. Red dots are σ of each point. (a) Intensity versus β for $|\lambda| < 3°$. (b) Same for $|\lambda| < 15°$.

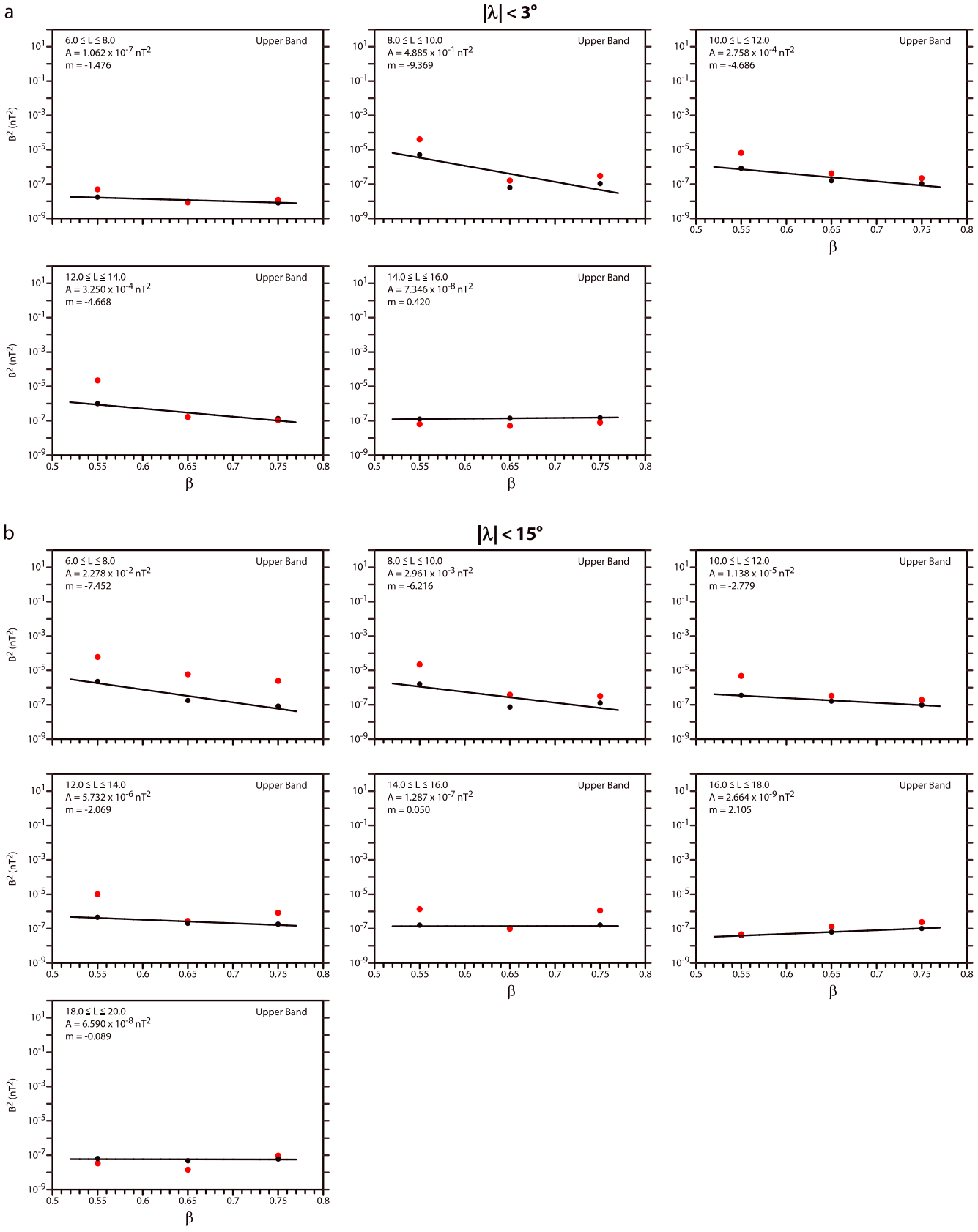

Figure 7. Same as Figure 6 but now for upper band chorus.

may mean that the influence of wave-particle interactions with whistler mode emission near Ganymede is rapidly distributed in the Jovian magnetosphere and warrants further study.

Intensity levels at Jupiter are typically about an order of magnitude greater than those observed at Saturn [cf. *Menietti et al*., 2014], with a significantly larger distribution in *L*. The intensity levels and region of high occurrence rates at Jupiter are larger than those considered in global diffusive models of electron acceleration at Jupiter [cf. *Horne et al*., 2008; *Shprits et al*., 2012; *Woodfield et al*., 2014], suggesting that chorus wave-particle interactions at Jupiter may play an even greater role than earlier proposed. The orbital survey of the Galileo satellite is quite limited compared to the many orbits of the Cassini mission but will be supplemented by the Juno mission at Jupiter.

Acknowledgments

We wish to thank J. Barnholdt for clerical assistance and J. Chrisinger for help with many figures. J.D.M. acknowledges support from JPL contract 1415150 and NASA grant NNX11AM36G. R.B.H. and E. E.W. are funded through STFC grant ST/M00130X/1. R.B.H. is funded by the UK Natural Environment Research Council. M.S.-S.P. acknowledges research carried out at the Jet Propulsion Laboratory, California Institute of Technology, under a contract with the National Aeronautics and Space Administration. Galileo PWS data are archived in calibrated, full resolution at the NASA Planetary Data System website: https://pds.nasa.gov/ds-view/pds/viewDataset.jsp?dsid=GO-J-PWS-2-REDR-LPW-SA-FULL-V1.0.

References

Bolton, S. J., R. M. Thorne, D. A. Gurnett, W. S. Kurth, and D. J. Williams (1997), Enhanced whistler-mode emissions: Signatures of interchange motion in the Io torus, *Geophys. Res. Lett.*, *24*, 2123–2126, doi:10.1029/97GL02020.

Connerney, J. E. P., N. F. Ness, and M. H. Acuña (1982), Zonal harmonic model of Saturn's magnetic field from Voyager 1 and 2 observations, *Nature*, *298*, 44–46, doi:10.1038/298044a0.

Connerney, J. E. P., M. H. Acuña, and N. F. Ness (1983), Currents in Saturn's magnetosphere, *J. Geophys. Res.*, *88*, 8779–8789, doi:10.1029/JA088iA11p08779.

Cowley, S. W. H., and E. J. Bunce (2003), Modulation of Jovian middle and magnetosphere currents and auroral precipitation by solar wind-induced compressions and expansions of the magnetosphere: Initial conditions and steady state, *Planet. Space Sci.*, *51*, 31, doi:10.1016/S0032-0633(02)00130-7.

Divine, N., and H. B. Garrett (1983), Charged particle distributions in Jupiter's magnetosphere, *J. Geophys. Res.*, *88*, 6889–6903, doi:10.1029/JA088iA09p06889.

Gurnett, D. A., W. S. Kurth, R. R. Shaw, A. Roux, R. Gendrin, C. F. Kennel, F. L. Scarf, and S. D. Shawhan (1992), The Galileo plasma wave investigation, *Space Sci. Rev.*, *60*, 341–355, doi:10.1007/BF00216861.

Gurnett, D. A., W. S. Kurth, A. Roux, S. J. Bolton, and C. F. Kennel (1996), Evidence for a magnetosphere at Ganymede from plasma-wave observations by the Galileo spacecraft, *Nature*, *384*, 535–537, doi:10.1038/384535a0.

Hartley, D. P., Y. Chen, C. A. Kletzing, M. H. Denton, and W. S. Kurth (2015), Applying the cold plasma dispersion relation to whistler mode chorus waves: EMFISIS wave measurements from the Van Allen Probes, *J. Geophys. Res. Space Physics*, *120*, 1144–1152, doi:10.1002/2014JA020808.

Hill, T. W., A. J. Dessler, and C. K. Goertz (1983), Jovian magnetospheric models, in *Physics of the Jovian Magnetosphere*, edited by A. J. Dessler, pp. 353 , Cambridge Univ. Press, New York.

Horne, R. B., and R. M. Thorne (1998), Potential waves for relativistic electron scattering and stochastic acceleration during magnetic storms, *Geophys. Res. Lett.*, *25*, 3011–3014, doi:10.1029/98GL01002.

Horne, R. B., and R. M. Thorne (2003), Relativistic electron acceleration and precipitation during resonant interactions with whistler-mode chorus, *Geophys. Res. Lett.*, *30*(10), 1527, doi:10.1029/2003GL016973.

Horne, R. B., et al. (2005), Wave acceleration of electrons in the Van Allen radiation belts, *Nature*, *437*, 227–230, doi:10.1038/nature03939.

Horne, R. B., M. M. Thorne, S. A. Glauert, J. D. Menietti, Y. Y. Shprits, and D. A. Gurnett (2008), Gyro-resonant electron acceleration at Jupiter, *Nat. Phys.*, *4*, 301–304, doi:10.1038/nphys897.

Hospodarsky, G. B., T. F. Averkamp, W. S. Kurth, D. A. Gurnett, J. D. Menietti, O. Santolík, and M. K. Dougherty (2008), Observations of chorus at Saturn using the Cassini Radio and Plasma Wave Science instrument, *J. Geophys. Res.*, *113*, A12206, doi:10.1029/2008JA013237.

Hospodarsky, G. B., K. Sigsbee, J. S. Leisner, J. D. Menietti, W. S. Kurth, D. A. Gurnett, C. A. Kletzing, and O. Santolík (2012), Plasma wave observations at Earth, Jupiter, and Saturn, in *Dynamics of the Earth's Radiation Belts and Inner Magnetosphere*, edited by D. Summers et al., pp. 415–430 , AGU, Washington, D. C., doi:10.1029/2012GM001342.

Katoh, Y., F. Tsuchiya, Y. Miyoshi, A. Morioka, H. Misawa, R. Ujiie, W. S. Kurth, A. T. Tomás, and N. Krupp (2011), Whistler mode chorus enhancements in association with energetic electron signatures in the Jovian magnetosphere, *J. Geophys. Res.*, *116*, A02215, doi:10.1029/2010JA016183.

Kennel, C. F., and F. Engelmann (1966), Velocity space diffusion from weak plasma turbulence in a magnetic field, *Phys. Fluids*, *9*, 2377–2388, doi:10.1063/1.1761629.

Kivelson, M. G., K. K. Khurana, J. D. Means, C. T. Russell, and R. C. Snare (1992), The Galileo magnetic field investigation, *Space Sci. Rev.*, *60*, 357–383, doi:10.1007/BF00216862.

Kurth, W. S., D. A. Gurnett, A. Roux, and S. J. Bolton (1997), Ganymede: A new radio source, *Geophys. Res. Lett.*, *24*, 2167–2170, doi:10.1029/97GL02249.

Lerche, I. (1968), Quasilinear theory of resonant diffusion in a magneto-active, relativistic plasma, *Phys. Fluids*, *11*, 1720–1727, doi:10.1063/1.1692186.

Louarn, P., C. P. Paranicas, and W. S. Kurth (2014), Global magnetodisk disturbances and energetic particle injections at Jupiter, *J. Geophys. Res. Space Physics*, *119*, 4495–4511, doi:10.1002/2014JA019846.

Mauk, B. H., D. J. Williams, and R. W. McEntire (1997), Energy-time dispersed charged particle signatures of dynamic injections in Jupiter's inner magnetosphere, *Geophys. Res. Lett.*, *24*, 2949–2952, doi:10.1029/97GL03026.

Mauk, B. H., D. J. Williams, R. W. McEntire, K. K. Khurana, and J. G. Roederer (1999), Storm-like dynamics of Jupiter's inner and middle magnetosphere, *J. Geophys. Res.*, *104*, 22,759–22,778, doi:10.1029/1999JA900097.

Menietti, J. D., R. B. Horne, D. A. Gurnett, G. B. Hospodarsky, C. W. Piker, and J. B. Groene (2008a), A survey of Galileo plasma wave instrument observations of Jovian whistler-mode chorus, *Ann. Geophys.*, *26*, 1819–1828, doi:10.5194/angeo-26-1819-2008.

Menietti, J. D., O. Santolík, A. M. Rymer, G. B. Hospodarsky, A. M. Persoon, D. A. Gurnett, A. J. Coates, and D. T. Young (2008b), Analysis of plasma waves observed within local plasma injections seen in Saturn's magnetosphere, *J. Geophys. Res.*, *113*, A05213, doi:10.1029/2007JA012856.

Menietti, J. D., Y. Y. Shprits, R. B. Horne, E. E. Woodfield, G. B. Hospodarsky, and D. A. Gurnett (2012), Chorus, ECH, and Z mode emissions observed at Jupiter and Saturn and possible electron acceleration, *J. Geophys. Res.*, *117*, A12214, doi:10.1029/2012JA018187.

Menietti, J. D., T. F. Averkamp, J. B. Groene, R. B. Horne, Y. Y. Shprits, E. E. Woodfield, G. B. Hospodarsky, and D. A. Gurnett (2014), Survey analysis of chorus intensity at Saturn, *J. Geophys. Res. Space Physics*, *119*, 8415–8425, doi:10.1002/2014JA020523.

Meredith, N. P., R. B. Horne, A. Sicard-Piet, D. Boscher, K. H. Yearby, W. Li, and R. M. Thorne (2012), Global model of lower band and upper band chorus from multiple satellite observations, *J. Geophys. Res.*, *117*, A10225, doi:10.1029/2012JA017978.

Pontius, D. H., Jr., T. W. Hill, and M. E. Rassbach (1986), Steady state plasma transport in a corotation-dominated magnetosphere, *Geophys. Res. Lett.*, *13*, 1097–1100, doi:10.1029/GL013i011p01097.

Santolík, O., et al. (2010), Wave-particle interactions in the equatorial source region of whistler-mode emissions, *J. Geophys. Res.*, *115*, A00F16, doi:10.1029/2009JA015218.

Shprits, Y. Y., J. D. Menietti, X. Gu, K. C. Kim, and R. B. Horne (2012), Gyroresonant interactions between the radiation belt electrons and whistler mode chorus waves in the radiation environments of Earth, Jupiter, and Saturn: A comparative study, *J. Geophys. Res.*, *117*, A11216, doi:10.1029/2012JA018031.

Stix, T. H. (1992), *Waves in Plasmas*, Am. Inst. of Phys., New York.

Thorne, R. M. (2010), Radiation belt dynamics: The importance of wave-particle interactions, *Geophys. Res. Lett.*, *37*, L22107, doi:10.1029/2010GL044990.

Thorne, R. M., T. P. Armstrong, S. Stone, D. J. Williams, R. W. McEntire, S. J. Bolton, D. A. Gurnett, and M. G. Kivelson (1997), Galileo evidence for rapid interchange transport in the Io torus, *Geophys. Res. Lett.*, *24*, 2131–2134, doi:10.1029/97GL01788.

Thorne, R. M., et al. (2013), Evolution and slow decay of an unusual narrow ring of relativistic electrons near L ~ 3.2 following the September 2012 magnetic storm, *Geophys. Res. Lett.*, *40*, 3507–3511, doi:10.1002/grl.50627.

Woodfield, E. . E., R. . B. Horne, S. . A. Glauert, J. . D. Menietti, and Y. . Y. Shprits (2013), Electron acceleration at Jupiter: Input from cyclotron-resonant interaction with whistler-mode chorus waves, *Ann. Geophys.*, *31*, 1619–1630, doi:10.5194/angeo-31-1619-2013.

Woodfield, E. . E., R. . B. Horne, S. . A. Glauert, J. . D. Menietti, and Y. . Y. Shprits (2014), The origin of Jupiter's outer radiation belt, *J. Geophys. Res. Space Physics*, *119*, 3490–3502, doi:10.1002/2014JA019891.